Technical Report

A. Significance and Objectives

Data from the PBO continuous GPS network allowed Argus et al. [2014], Amos et al. [2014] and Borsa et al. [2014] to document crustal deformation in California associated with seasonal changes in hydrospheric surface loads (groundwater, surface water, snow), as well as regional uplift due to the recent drought in the western U.S. This dense network of continuous GPS stations allows real-time monitoring of crustal water storage. Annual vertical and horizontal displacement amplitudes of GPS stations in the Sierra Nevada and California Coast Ranges are on the order of 1-5 mm and 0.5-2 mm, respectively [*Amos et al.*, 2014]. Water loss due to drought conditions in recent years resulted in longer-term uplift of areas surrounding the Central Valley at rates of up to ~5 mm/yr. In contrast, stations in the Central Valley and other young sedimentary basins rise and fall with the groundwater level in the aquifer below due to the poroelastic response to changes in water head [*Chaussard et al.*, 2014].

Knowledge of what governs the timing of earthquakes is essential to understanding the nature of the earthquake cycle and to determining time-dependent earthquake hazard, yet the variability and controls of earthquake occurrences are not well established. If slight changes in static stress influence the timing of earthquakes, either promoting or discouraging nucleation, then one could expect that earthquakes will occur more often during periods of preferential surface loading conditions. Seasonal crustal stress variations can result from hydrospheric and atmospheric surface loads [*Amos et al.*, 2014; *Dong et al.*, 2002; *Gao et al.*, 2000; *Heki*, 2003; *Holzer*, 1979; *Namias*, 1989], fluctuations of subsurface pore fluid pressures [*Christiansen et al.*, 2007; *Hainzl et al.*, 2013], and thermoelastic strains from atmospheric temperature variations [*Ben-Zion and Allam*, 2013]. A number of studies suggest that seismicity correlates with seasonal forcing [*Bettinelli et al.*, 2008; *Christiansen et al.*, 2007; *Gao et al.*, 2000; *Hainzl et al.*, 2013; *Heki*, 2003; *Pollitz et al.*, 2013]. In California, seasonal cycles of snow and water loads in the Sierra Nevada and Central Valley [*Amos et al.*, 2014; *Argus et al.*, 2014] may help drive such periodic seismicity patterns [*Christiansen et al.*, 2007; *Gao et al.*, 2000; *Zaliapin and Ben-Zion*, 2013]. The lack of observational documentation of the statistical significance of such modulation in natural earthquake populations has so far limited the consideration of small stress changes in time-dependent earthquake forecasting.

Simple models of stress changes on the San Andreas (SAF) and other nearby faults from the associated elastic deformation suggest seasonal stress cycles of up to ~1 kPa [*Amos et al.*, 2014], comparable to those associated with the short-period solid Earth tides [*Thomas et al.*, 2012]. While modest compared to annual interseismic fault loading rates of 5-50 kPa/yr [*Parsons*, 2006; *Smith and Sandwell*, 2006], the long period of the stress cycles (comparable to duration of earthquake nucleation) may be expected to allow for detectable modulation of crustal seismicity from these seasonal load cycles [*Beeler and Lockner*, 2003]. Detailed investigations of focal mechanisms in southern California reveal a heterogeneous stress field and variations in faulting style [*Yang and Hauksson*, 2013] that need to be considered when investigating the effect of applied stress transients on fault activity. In this study we rigorously characterize the seasonal periodicity in the seismicity catalog, model seasonal deformation and stress, and evaluate changes in location and mechanisms of earthquakes to better understand the effects of small stress changes resulting from varying surface loads in California.

The project results spatially and temporally characterize the near surface water storage using geodetic observations and modeling to fully describe the associated stress changes from the annual water storage, atmosphere pressure, temperature variations, ocean tides, solid Earth body tides, and Earth's rotation axis pole tides. The stress analysis is used to test the sensitivity of earthquake occurrence with respect to small external stressing due to seasonal changes in near surface loading cycles. Completed is the analysis of statistical significance of observed periodicities in California seismicity records [*Dutilleul et al.*, 2015], hydrospheric load modeling to describe the temporally changing stresses on active fault structures that modulate low magnitude seismicity [*Johnson et al.*, 2017b], and the aggregate stressing contribution from atmospheric, hydrospheric, thermal, and tidal loads for an analysis of the stress changes with respect to the ambient stress field and local fault geometry [*Johnson et al.*, 2017a]. All results in the study have been published in refereed journals and presented at conferences listed 1G.

B. Statistical Significance of Detected Periodicity in CA Earthquake Occurrence

Periodicities in earthquake occurrence may represent seasonally varying conditions due to changes in hydrospheric loads. We explore seismicity catalogs in two regions of CA, one near the central SAF and the second in the Sierra Nevada – Eastern California Shear Zone (SN-ECSZ), for periodic behavior using three independent statistical tests. To ensure a robust analysis, we test 26 years of M≥2.5 catalog data and apply two declustering methods. The first is the [*Reasenberg*, 1985] method developed for northern and central California. The second is a spatial-temporal ETAS model that estimates the probability that an event is a background earthquake [*Zhuang et al.*, 2002]. Both methods are widely used and appropriate for the purpose of testing the regions of interest. We consider both the original earthquake catalogs as well as subsets made of declustered events that separate dependent seismic activity produced by fault interaction, including foreshocks and aftershocks, from independent background earthquakes, including mainshocks and single events [*van Stiphout et al.*, 2012], thereby testing a total of six catalogs. We examine to what degree the choice of declustering algorithm [*Reasenberg*, 1985; *Zhuang et al.*, 2002] affects the results of our analysis. The statistical analyses are described in last year's technical report and full details are published in [*Dutilleul et al.*, 2015].

Near Parkfield, CA we find strong evidence for annual periods in earthquake occurrence, consistent with previous results suggesting seasonal modulation of seismicity [*Christiansen et al.*, 2007]. The results indicate statistically significant periods of about 4-, 6-, and 12-months for seismicity located on the SAF near Parkfield. For this region we find peak earthquake occurrence in the dry fall months of August and September and a secondary peak in activity in April. Similarly, in the SN-ECSZ we find a statistically significant annual period, as well as a ~14 month period that we specifically test for in order to consider the period of pole-tide induced stresses. The results indicate the declustering methods reduce the periodic component resolved in the time series, but do not produce a Poissonian process since we are able to resolve similar periods when compared to the original time series.

We find that there is significant annual periodicity in earthquakes along the central SAF and adjacent Coast Ranges that appears to reflect seasonal loading from hydrospheric and tidal loads. We explore the phase and amplitude information of periodic sources of stress including the pole tides, annual and semi-annual tides, and annual hydrological load cycles. The pole tides and the semi-annual and annual tides are estimated following [*Shen et al.*, 2005] and *Agnew* [1997], respectively, and both oscillate at the same phase for periods of interest in California, with the amplitude determined by the latitude. Modeled peak-to-trough shear-stress amplitudes on the CSAF from the pole-tides and tides are of order 100 Pa and combine to produce sub-equal peaks of stress encouraging right-lateral slip in the spring and fall. Fault-normal pole-tide stress on the CSAF has an amplitude of > 700 Pa, with annual components of ~200 Pa and peak tension in the spring. Fault-normal peak-to-trough stress amplitude from the tides is only 30 Pa. Normal-stress cycles from seasonal hydrological unloading have been estimated to be of order ~1000 Pa peak-to-trough, with greatest tensile stress in October during the drier months. This suggests that the fall peak in earthquake occurrence is due to the dominantly fault-normal stress cycles of hydrological surface loads, while the second peak in the spring may be related to stress cycles from the pole-tide and tidal contributions, which indicate a peak shear stress in March and September. The occurrence of two peaks in seismicity at times when the normal stress is favorable for fault unloading conditions would suggest the fault is encouraged to slip by shear stress change of order 100 Pa, considerably less than static or dynamic stress changes typically associated with earthquake triggering. The modulation of seismicity with a period of one-year supports our hypothesis of seasonal loading and warrants our continued efforts to model the seasonal deformation associated with these time varying loads.

C. Time Varying Stresses on the Community Fault Model and Focal Mechanism Catalog

Modeling the time-dependent surface loading allows us to calculate the expected deformation from the addition or removal of mass from the Earth's surface using the near-surface water storage derived from vertical GPS displacements. The equivalent water storage is inverted from cGPS and represents the volume mass change in the hydrosphere that extends from 32˚N – 42.5˚N and 125˚W – 115˚W on a 0.25˚x0.25˚ grid and is resolved for a monthly time-series between 2006-2014. Additionally, we estimate surface mass changes from the atmosphere and ocean tides using global reanalysis models, the

thermoelastic stresses from annual temperature cycles, and stresses generated in the crust from Earth body tides due to celestial interaction and pole tides from changes in rotation rate. All surface mass estimates are used as a model input to calculate the deformation at both the surface and seismogenic depths (8 km). We implement an elastic mechanical model on a spherically stratified Earth model based on the preliminary reference Earth model (PREM) and generate a time-series of the deformation in the near surface that corresponds to the spatially varying distributed water storage, atmosphere pressure, and ocean tides. The static displacements are calculated using a modified version of STATIC1D [*Pollitz*, 1996; 1997] that is adapted for a vertical force at the surface and calculates the equations of static equilibrium. The calculated surface displacements are used to validate the model by comparing to the GPS time series. Tidal and thermal stresses are estimated independently using analytical solutions [*Agnew*, 1997; *Ben-Zion and Leary*, 1986; *Shen et al.*, 2005] to produce time series compatible with the surface load induced stress changes. The deformation at 8 km depth is used to estimate the stress changes for CA faults.

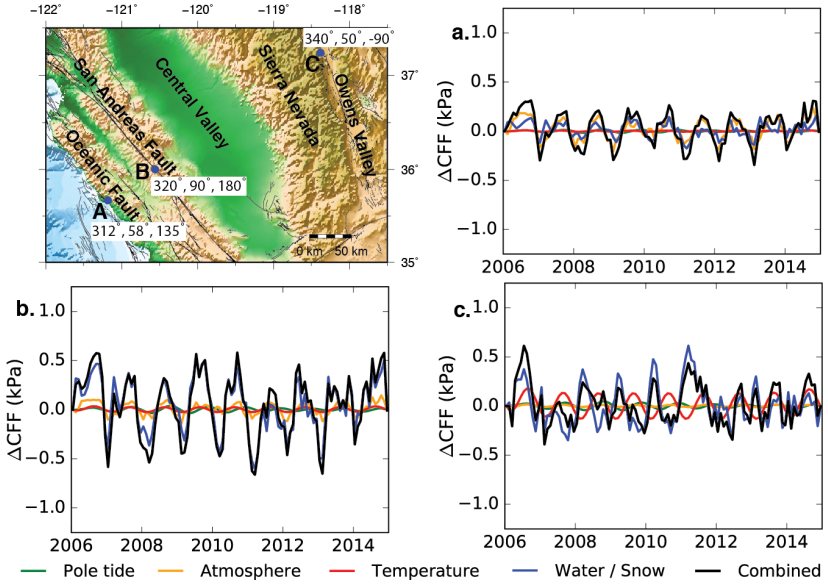

Figure 1. The location and the orientation of three faults are shown with the strike, dip, and rake directions for (a) the Oceanic Fault (-121.18, 35.67) near San Simeon, CA, (b) the central San Andreas Fault (-120.56, 36.00) near Parkfield, CA, and (c) the eastern Sierra range front normal fault in Owens Valley (-118.38, 37.34). The corresponding curves show the Coulomb stress (μ=0.4) change during the study period for the four largest loading sources and the combined total [*Johnson et al.,* 2017a].

The induced stress changes from hydrospheric, atmospheric, and tidal loading are computed for the fault geometry in the SCEC Community Fault Model [Field et al., 2013] and using focal mechanisms in the study region to resolve site-specific time-varying stresses throughout California. The fault model provides the location and the average strike, dip, and rake for CA faults. This allows high spatial and temporal sampling of transient deformation on these active structures. The stress time-series are shown at three locations spaced along a 300 km transect across central and eastern California for faults with different geometries (Figure 1). The faults selected show how the geometry and seasonal stresses vary across the region. This subsample of faults does not represent the full complexity of the varying fault geometry in the study area but does highlight the spatial heterogeneity of both the faults and loading cycles. Figure 2 shows the average annual peak-to-peak Coulomb stress (μ=0.4) change from the four dominant loads with the day-of-year for the maximum stress change. Along the Coast Ranges the maximum stress change is between 0.5 – 1.0 kPa and generally is at the maximum late in the year from August through October. An approximately 4-month difference is observed for many faults in the eastern Sierra Nevada, which have an annual stress changes < 1.0 kPa and experience the greatest increase in Coulomb stress during the early summer months.

We utilize the background stress orientation (Figure 3) derived from the focal mechanism catalog and assess the timing of events in the declustered hypocentral catalog. The assumption is all the earthquakes located in the volume of each grid patch experience the same seasonal stress perturbations. We quantify the percent excess seismicity (N_{Ex}) using 1.0 kPa stress intervals centered on zero for the resolved stress amplitude. The excess seismicity results indicate weak correlations with the background stress perturbations. Our results indicate a correlation with the change in mean normal stress. A plausible scenario

is an increase or reduction in pore pressure on faults as fluids migrate through the crust during an annual loading cycle, thereby increasing or decreasing the slip potential on a fault plane, respectively. Fluid mobilization would also introduce a time lag from the peak stress change to the onset of seismicity and is not explored in this study. Details of all the findings in the study are published in [*Johnson et al.*, 2017a].

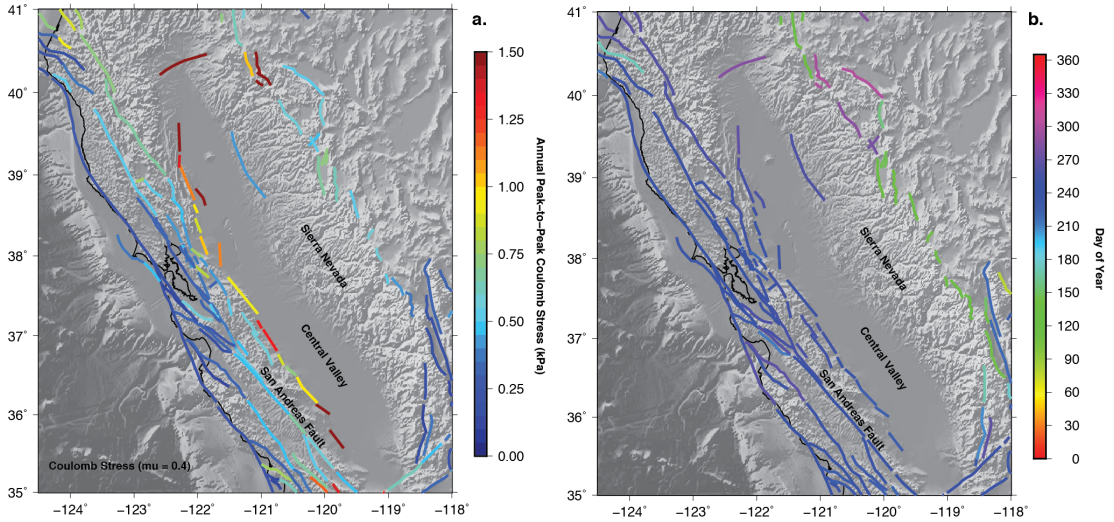

Figure 2. (a) The average annual peak-to-peak Coulomb stress (μ=0.4) change from the 4 largest loads (hydrological, atmosphere, pole-tides, and thermal) is shown on the UCERF3 fault model geometry with (b) the day of year of the peak stress. The aggregate stresses account for the phase differences in the loading cycles and provide a representative description of the seasonal stress change [*Johnson et al.,* 2017a].

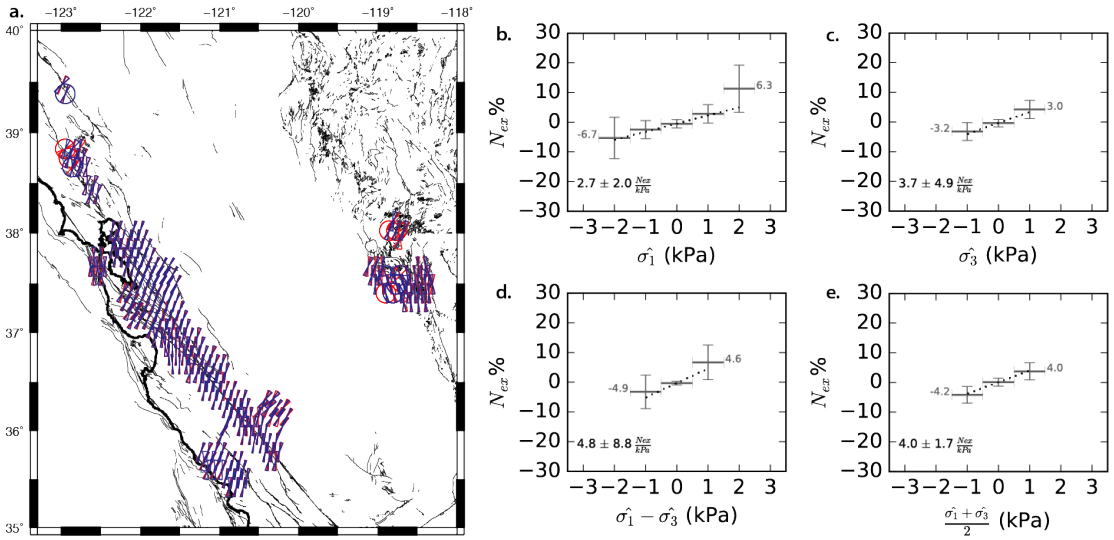

Figure 3. Seasonal stress tensor orientation comparison for the time intervals of May – October and November – April. (a) The azimuth of S_{Hmax} shown with 95% confidence intervals for winter (blue) and summer (red) months. The percent excess seismicity for normal-stress changes in the (b) σ_1 orientation, (c) σ_3 orientation, (d) for the differential stress (σ_1-σ_3), and (e) the mean normal stress. The horizontal bar shows the stress interval, the vertical error bars represent the 95% confidence interval. Negative normal-stress-change values indicate increased compression and negative differential stress changes increase loads on favorable oriented faults. The numeric values at the end member bins represent the minimum and maximum range of the stresses calculated for all the events. The trend of the best-fit line is shown in the bottom left of each panel with the 2-sigma error and shown as the dashed line [*Johnson et al.,* 2017a].

Additionally, we look at the focal plane orientation of events and explore the stresses resolved for the fault plane orientation and the ambient stress field orientation [*Hardebeck and Michael*, 2006]. The focal

mechanism results are produced using the first motion phase arrivals available through the Northern California Earthquake Data Center (http://ncedc.org) with the FPFIT algorithm [Reasenberg and Oppenheimer, 1985] for M≥2 events between 2006 through 2014 for northern and central California. The algorithm uses a grid search method to minimize the misfit of the P-wave first-motion polarities using the available phase information. To ensure high-quality focal mechanisms we require a minimum of 25 observations to calculate a solution and eliminate many solutions that are below our standards. We remove all focal mechanism solutions that do not converge, have a station distribution ratio <0.55, or if the strike, dip, and rake error is >35˚. The station distribution ratio is the best quantitative measure of the quality of the FPFIT solution [*Kilb and Hardebeck*, 2006].

The focal mechanisms are separated into populations of dip-slip containing the reverse, normal, and oblique events (N=2,345) and strike-slip (N=1,344) events. A positive trend is observed for the shear stress amplitude and the strike-slip events of 22.5 ± 18.2 N_{ex}/kPa (at 95% confidence) between -1.1 and 1.6 kPa, indicating a seismic response to the peak shear amplitude. The dip-slip events exhibit a response to the shear stressing rate with a positive trend of 12.5 ± 5.9 N_{ex}/kPa/yr, ranging from -11.8 to 26.7 kPa/yr. Excess events are not observed for the strike-slip events from an increase in the shear stressing rate and similarly the dip-slip events do not show excess seismicity as the shear stress amplitude increases. The N_{Ex} values indicate that earthquakes are occurring at different times of the shear stress cycle for different fault types, suggesting that the strike-slip events are mechanically different from the dip-slip population. Full details of the analysis are published in [*Johnson et al.*, 2017b] for additional information.

D. Significant Findings

The 3-year project consists of four primary components: (i) evaluate the statistical significance of detected periods in seismicity catalogs for events located along the SAF and in the SN-ECSZ, (ii) develop elastic deformation models of monthly surface loads, (iii) evaluate the degree of correlation between model stress cycles and seismicity taking into consideration the variable amplitude of stress cycles, the orientation of transient load stress with respect to the background stress field, and the geometry of active faults revealed by focal mechanisms, and (iv) analyze loading cycles of additional natural cycles that produce stress changes on fault systems. All components of the project are complete and available in published journals listed in the SCEC Publications database. The findings in the first project component indicate significant annual periods in the seismicity records and provide the motivation for detailed modeling of the annual stress cycles. The second and third components are complete when considering hydrological loading cycles. We find seismicity occurring more often during periods of favorable stress conditions of focal plane orientations for M≥2.0 earthquakes. The fourth component is complete and details the stress changes from atmospheric, hydrospheric, thermal, and tidal loading cycles. The combined total periodic stresses are evaluated for the CFM geometry and with respect to the ambient stress field. The results do not indicate a resolvable change in the orientation of the stress tensors or the maximum horizontal stress direction, suggesting an observable change in seismicity is more likely from stress changes that align with the background stress. Seismicity rates are found to modestly increase during periods of reduced compressional mean normal stress.

E. References

Agnew, D. C. (1997), NLOADF: A program for computing ocean-tide loading, *Journal of Geophysical Research*, *102*(B3), 5109-5110, doi:10.1029/96jb03458.

Amos, C. B., P. Audet, W. C. Hammond, R. Bürgmann, I. A. Johanson, and G. Blewitt (2014), Contemporary uplift and seismicity in central California driven by groundwater depletion, *Nature*, *509*, 483-486, doi:10.1038/nature13275.

Argus, D. F., Y. Fu, and F. Landerer (2014), GPS as a high resolution technique for evaluating water resources in California, *Geophys. Res. Lett.*, *41*, doi: 10.1002/2014GL059570.

Beeler, N. M., and D. A. Lockner (2003), Why earthquakes correlate weakly with the solid Earth tides: Effects of periodic stress on the rate and probability of earthquake occurrence, *J. Geophys. Res.*, *108*(B8), doi:10.1029/2001jb001518.

Ben-Zion, Y., and A. A. Allam (2013), Seasonal thermoelastic strain and postseismic effects in Parkfield borehole dilatometers, *Earth Planet. Sci. Lett.*, *379*, doi:10.1016/j.epsl.2013.1008.1024.

Ben-Zion, Y., and P. Leary (1986), Thermoelastic strain in a half-space covered by unconsolidated material, *Bulletin of the Seismological Society of America*, *76*(5), 1447-1460.

Bettinelli, P., J.-P. Avouac, M. Flouzat, L. Bollinger, G. Ramillien, S. Rajaure, and S. Sapkota (2008), Seasonal variations of seismicity and geodetic strain in the Himalaya induced by surface hydrology, *Earth Planet. Sci. Lett.*, *266*, 332-344, doi:10.1016/j.epsl.2007.11.021.

Borsa, A. A., D. C. Agnew, and D. R. Cayan (2014), Ongoing drought-induced uplift in the western United States, *Science*, *345*(6204), 1587-1590.

Chaussard, E., R. Bürgmann, M. Shirzaei, E. Fielding, and B. Baker (2014), Predictability of hydraulic head changes and characterization of aquifer system and fault properties from InSAR-derived ground deformation, *J. Geophys. Res.*, *119*(8), 6572-6590, doi:10.1002/2014JB011266.

Christiansen, L. B., S. Hurwitz, and S. E. Ingebritsen (2007), Annual modulation of seismicity along the San Andreas Fault near Parkfield, CA, *Geophys. Res. Lett.*, *34*(L04306), doi:10.1029/2006GL028634.

Dong, D., P. Fang, Y. Bock, M. K. Cheng, and S. Miyazaki (2002), Anatomy of apparent seasonal variations from GPS-derived site position time series, *J. Geophys. Res.*, *107*(B4), doi:10.1029/2001JB000573.

Dutilleul, P., C. W. Johnson, R. Bürgmann, Y. Wan, and Z.-K. Shen (2015), Multifrequential periodogram analysis of earthquake occurrence: An alternative approach to the Schuster spectrum, with two examples in central California, *Journal of Geophysical Research: Solid Earth*, *120*(12), 8494-8515, doi:10.1002/2015JB012467.

Field, E. H., et al. (2013), Uniform California earthquake rupture forecast, version 3 (UCERF3) The time-independent model: U.S. Geological Survey Open-File Report 2013-1165, *California Geological Survey Special Report 228, and Southern California Earthquake Center Publication 1792*, 97p, *http://pubs.usgs.gov/of/2013/1165/*.

Gao, S. S., P. G. Silver, A. T. Linde, and I. S. Sacks (2000), Annual modulation of triggered seismicity following the 1992 Landers earthquake in California, *Nature*, *406*, 500-504.

Hainzl, S., Y. Ben-Zion, C. Cattania, and J. Wassermann (2013), Testing atmospheric and tidal earthquake triggering at Mt. Hochstaufen, Germany, *Journal of Geophysical Research: Solid Earth*, *118*(10), 5442-5452, doi:10.1002/jgrb.50387.

Hardebeck, J. L., and A. J. Michael (2006), Damped regional-scale stress inversions: Methodology and examples for southern California and the Coalinga aftershock sequence, *Journal of Geophysical Research*, *111*(B11), doi:10.1029/2005jb004144.

Heki, K. (2003), Snow load and seasonal variation of earthquake occurrence in Japan, *Earth and Planetary Science Letters*, *207*(1), 159-164, doi:10.1016/S0012-821X(02)01148-2.

Holzer, T. L. (1979), Elastic expansion of the lithosphere caused by groundwater depletion, *J .Geophys. Res.*, *84*, 4689–4698.

Johnson, C. W., Y. Fu, and R. Bürgmann (2017a), Stress Models of the Annual Hydrospheric, Atmospheric, Thermal, and Tidal Loading Cycles on California Faults: Perturbation of Background Stress and Changes in Seismicity, *Journal of Geophysical Research: Solid Earth*, *122*(12), 10,605-610,625, doi:10.1002/2017JB014778.

Johnson, C. W., Y. N. Fu, and R. Burgmann (2017b), Seasonal water storage, stress modulation, and California seismicity, *Science*, *356*(6343), 1161-1164, doi:10.1126/science.aak9547.

Kilb, D., and J. L. Hardebeck (2006), Fault Parameter Constraints Using Relocated Earthquakes: A Validation of First-Motion Focal-Mechanism Data, *Bulletin of the Seismological Society of America*, *96*(3), 1140-1158, doi:10.1785/0120040239.

Namias, J. (1989), Summer earthquakes in southern California related to pressure patterns at sea level and aloft, *J. Geophys. Res.*, *94*(B12), 17671-17679, doi:10.1029/89JB01463.

Parsons, T. (2006), Tectonic stressing in California modeled from GPS observations, *J. Geophys. Res.*, *111*(B03407), doi:10.1029/2005JB003946.

Pollitz, F. F. (1996), Coseismic deformation from earthquake faulting on a spherical earth, *Geophysical Journal International*, *125*, 1-14.

Pollitz, F. F. (1997), Gravitational viscoelastic postseismic relaxation on a layered spherical Earth, *Journal of Geophysical Research*, *102*(B8), 17921, doi:10.1029/97jb01277.

Pollitz, F. F., A. G. Wech, H. Kao, and R. Bürgmann (2013), Annual modulation of non-volcanic tremor in northern Cascadia, *J .Geophys. Res.*, *118*, doi:10.1002/jgrb.50181.

Reasenberg, P. (1985), Second-order moment of central California seismicity, 1969-82, *J .Geophys. Res.*, *90*, 5479-5495.

Reasenberg, P. A., and D. H. Oppenheimer (1985), FPFIT, FPPLOT, and FPPAGE: FORTRAN computer programs for calculating and displaying earthquake fault-plane solutions, *U.S. Geol. Surv. Open File Rept*, 85-739.

Shen, Z.-K., Q. Wang, R. Bürgmann, Y. Wan, and J. Ning (2005), Pole-Tide Modulation of Slow Slip Events at Circum-Pacific Subduction Zones, *Bulletin of the Seismological Society of America*, *95*(5), 2009-2015, doi:10.1785/0120050020.

Smith, B. R., and D. T. Sandwell (2006), A model of the earthquake cycle along the San Andreas Fault System for the past 1000 years, *J. Geophys. Res.*, *111*(B01405), doi:10.1029/2005JB003703.

Thomas, A. M., R. Bürgmann, D. R. Shelly, N. M. Beeler, and M. L. Rudolph (2012), Tidal triggering of low frequency earthquakes near Parkfield, CA: Implications for fault mechanics within the brittle-ductile transition, *J .Geophys. Res.*, *117*(B05301), doi:10.1029/2011JB009036.

van Stiphout, T., J. Zhuang, and D. Marsan (2012), Seismicity declustering, *Community Online Resource for Statistical Seismicity Analysis*, *Available at http://www.corssa.org*, doi:10.5078/corssa-52382934.

Yang, W., and E. Hauksson (2013), The tectonic crustal stress field and style of faulting along the Pacific North America Plate boundary in Southern California, *Geophysical Journal International*, *194*(1), 100-117, doi:10.1093/gji/ggt113.

Zaliapin, I., and Y. Ben-Zion (2013), Spatio-temporal evolution of seismic clusters in southern and central California, *SCEC Annual Meeting Poster presentation*.

Zhuang, J., Y. Ogata, and D. Vere-Jones (2002), Stochastic declustering of space-time earthquake occurrences, *J. Am. Stat. Assoc.*, *97*, 369-382.